Electronic Supplementary Material (ESI) for Materials Advances.
This journal is © The Royal Society of Chemistry 2022

Supporting Information (SI)
Lignin-derivable alternatives to petroleum-derived non-isocyanate polyurethane thermosets with enhanced toughness

Sampanna V. Mhatre,[a] Jignesh S. Mahajan,[a] Thomas H. Epps, III,[abc*] and LaShanda T. J. Korley[abc*]

[a]Department of Materials Science and Engineering, University of Delaware, Newark, Delaware 19716, USA

[b]Department of Chemical and Biomolecular Engineering, University of Delaware, Newark, Delaware 19716, USA

[c]Center for Research in Soft matter and Polymers (CRiSP), University of Delaware, Newark, Delaware 19716, USA

*Corresponding authors:
thepps@udel.edu
lkorley@udel.edu

Proton (^{1}H) Nuclear Magnetic Resonance (NMR) spectra for bisguaiacols in deuterated dimethyl sulfoxide (DMSO-d_6)

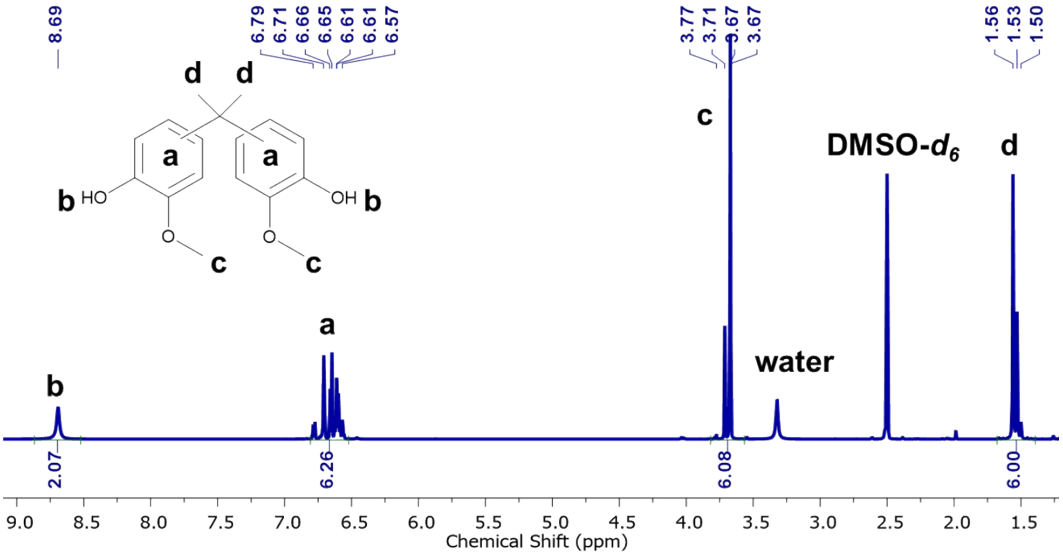

Figure S1. ^{1}H NMR spectrum of bisguaiacol A

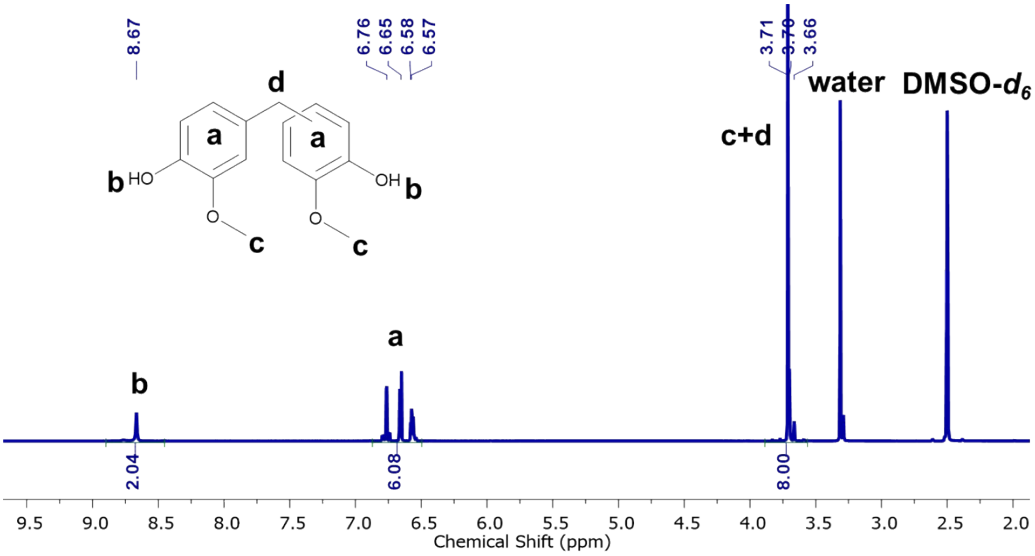

Figure S2. ^{1}H NMR spectrum of bisguaiacol F

^{1}H NMR spectra for diglycidyl ethers in DMSO-d_6

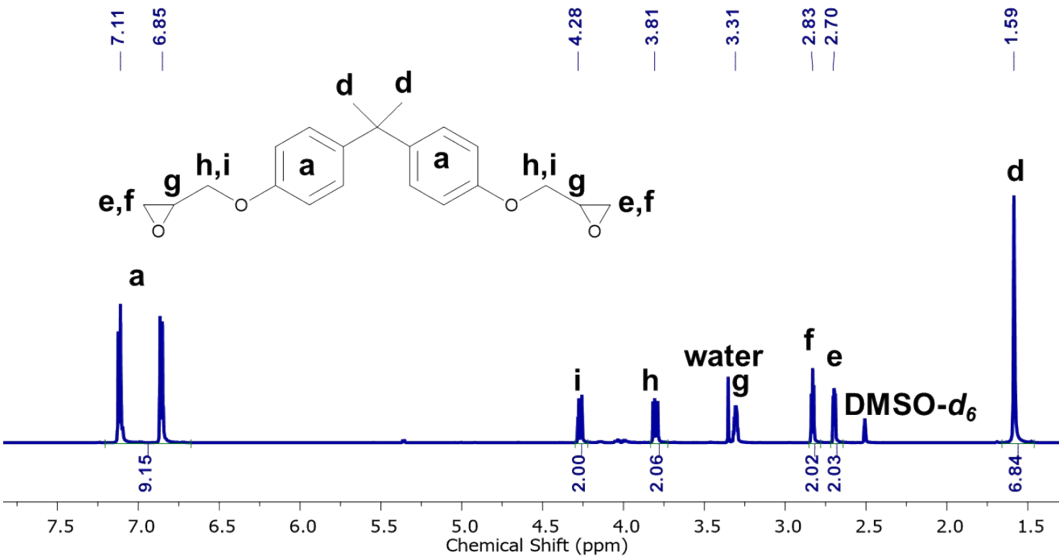

Figure S3. ^{1}H NMR spectrum of bisphenol A diglycidyl ether

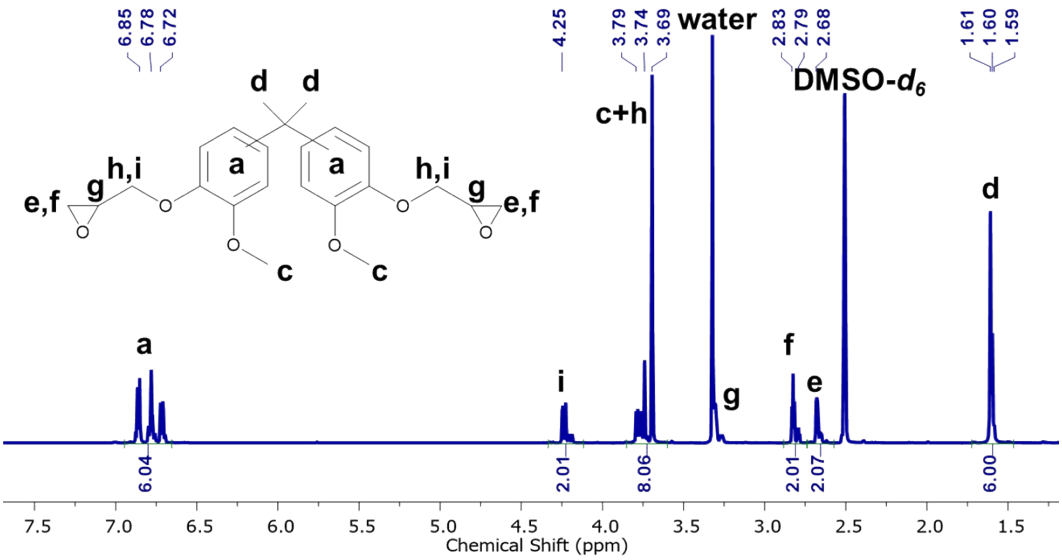

Figure S4. ^{1}H NMR spectrum of bisguaiacol A diglycidyl ether

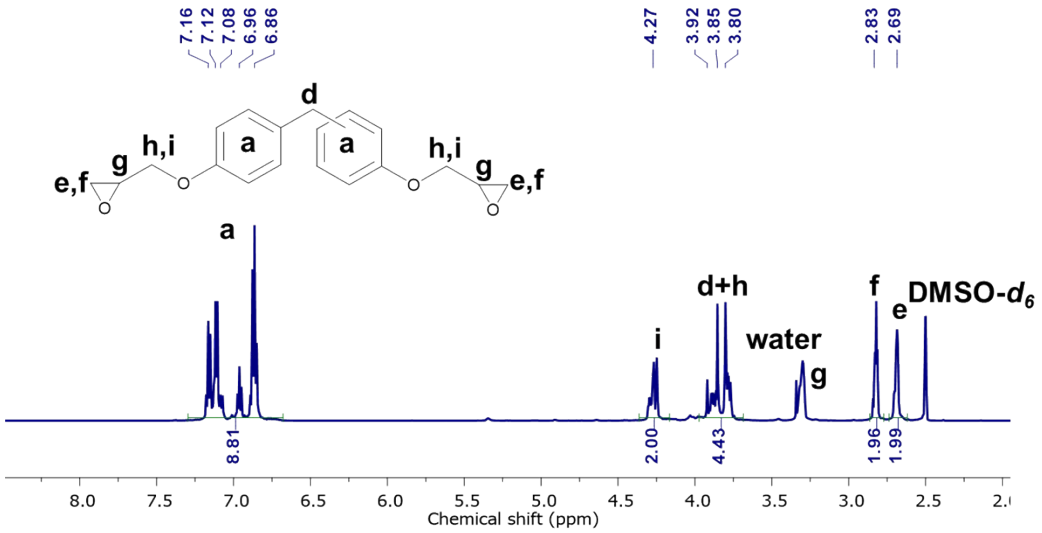

Figure S5. ^{1}H NMR spectrum of bisphenol F diglycidyl ether

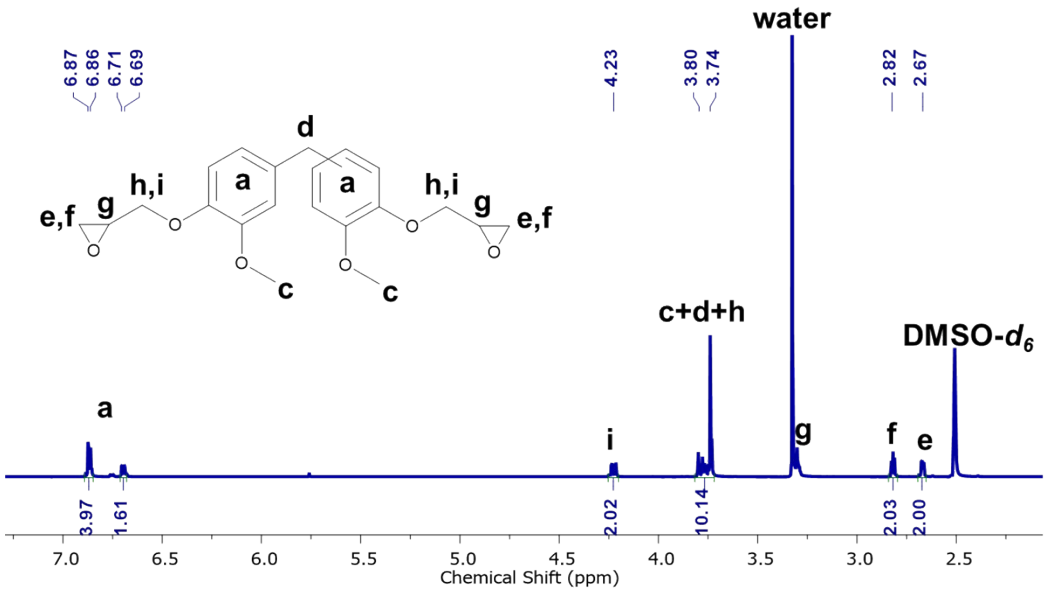

Figure S6. ^{1}H NMR spectrum of bisguaiacol F diglycidyl ether

^{1}H NMR spectra for cyclic carbonates in DMSO-d_6

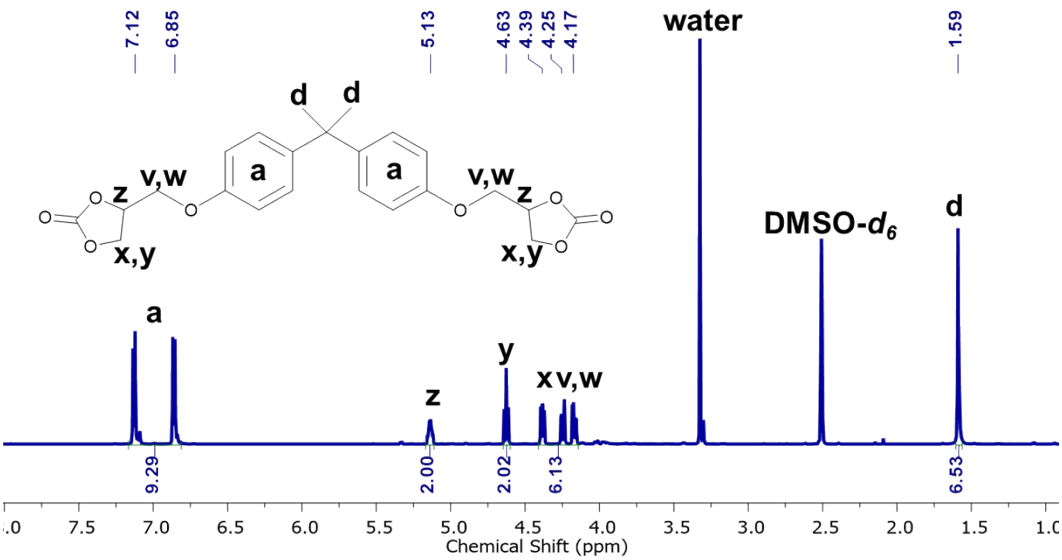

Figure S7. ^{1}H NMR spectrum of bisphenol A cyclic carbonate (BPACC)

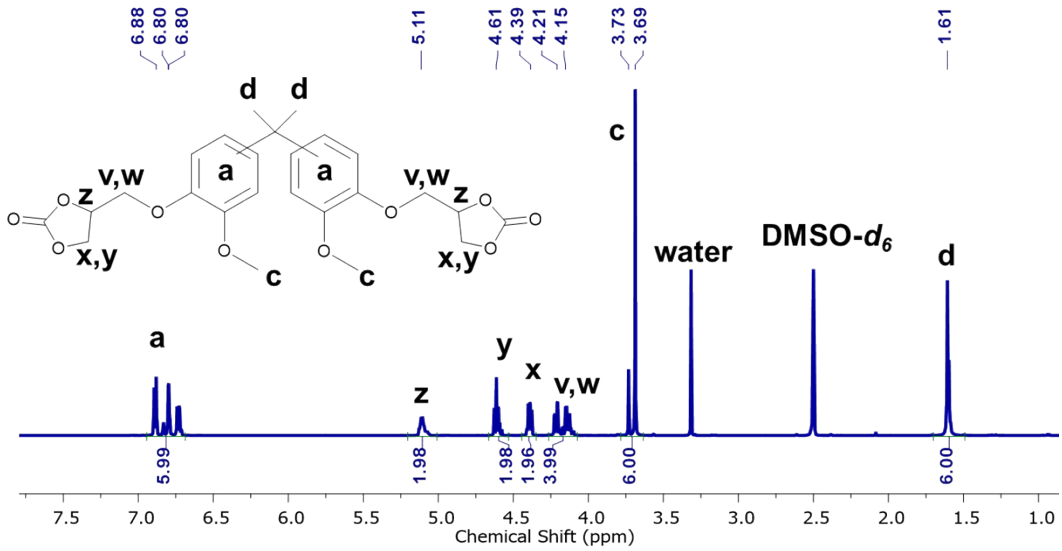

Figure S8. ^{1}H NMR spectrum of bisguaiacol A cyclic carbonate (BGACC)

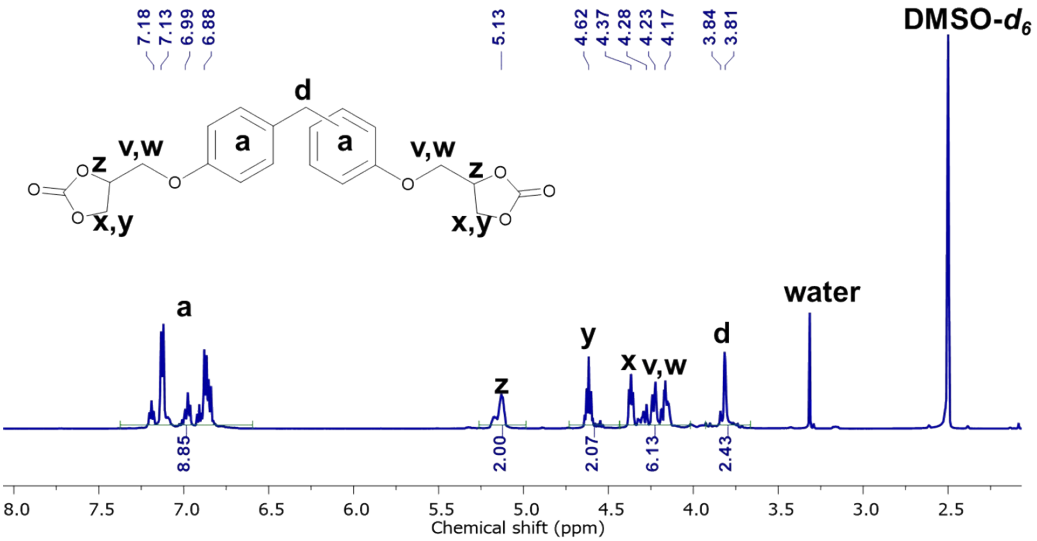

Figure S9. [1]H NMR spectrum of bisphenol F cyclic carbonate (BPFCC)

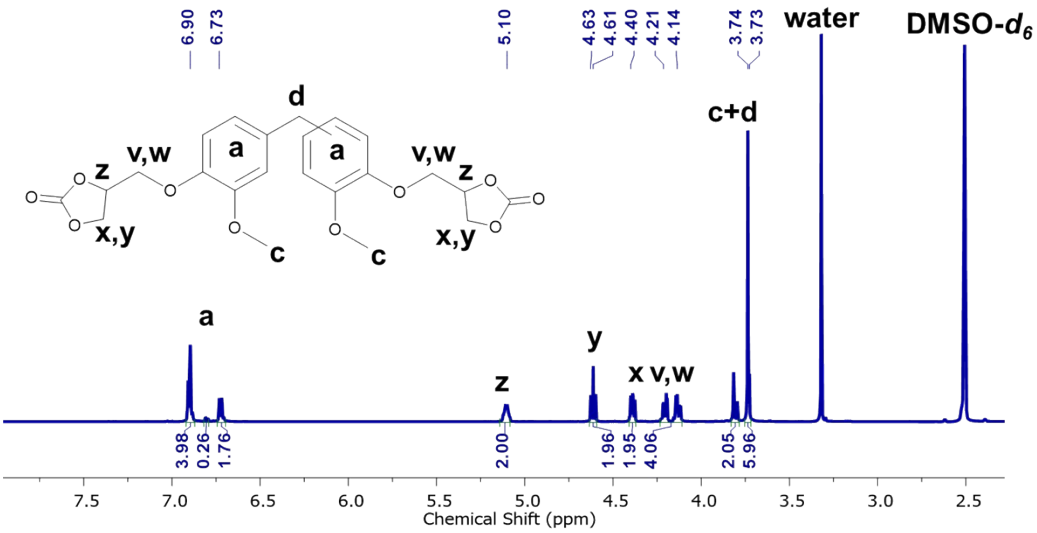

Figure S10. [1]H NMR spectrum of bisguaiacol F cyclic carbonate (BGFCC)

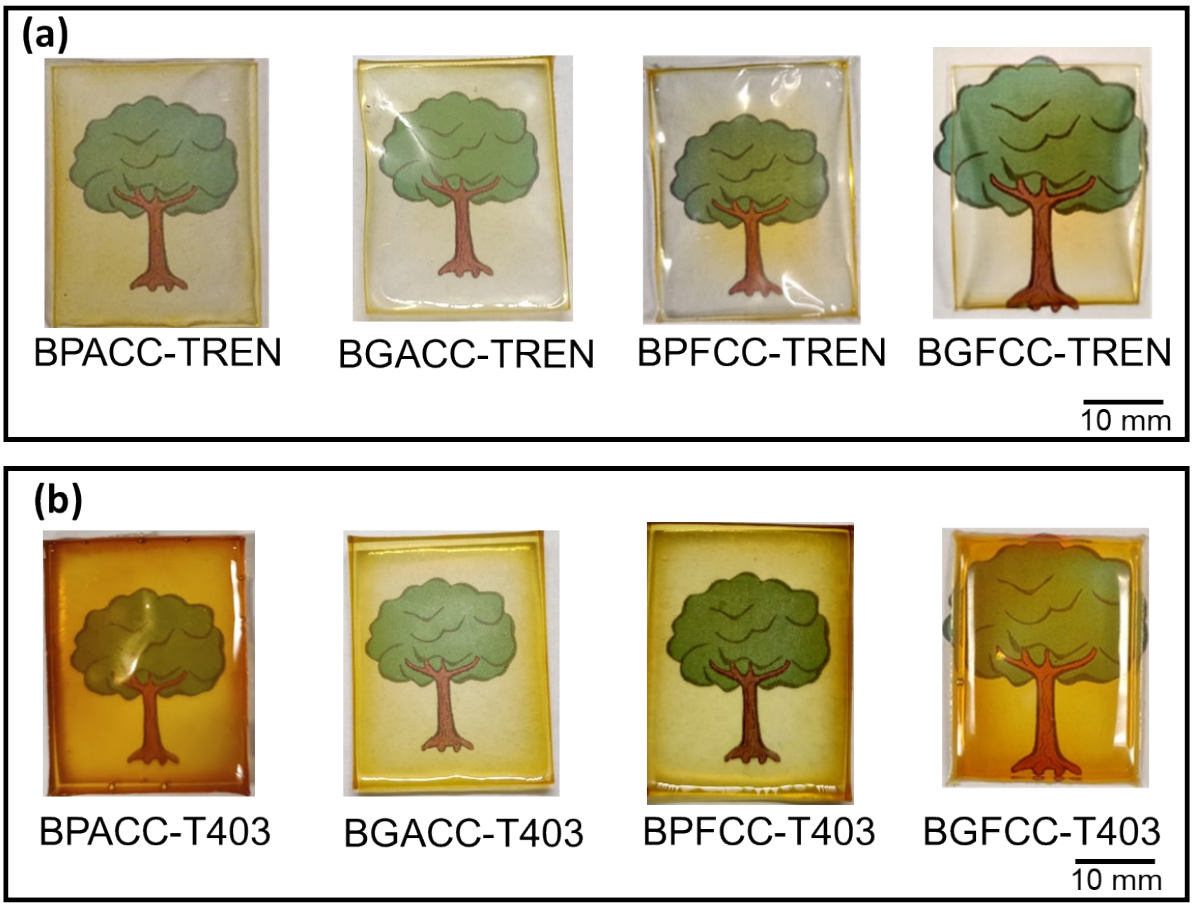

Figure S11. Photographs of non-isocyanate polyurethane (NIPU) networks, (a) crosslinked by tris(2-aminoethyl) amine (TREN) and (b) crosslinked by JEFFAMINE® T-403 (T403). The NIPUs were formed by the reaction of bifunctional cyclic carbonates and trifunctional amines dissolved in *N, N*-dimethylformamide. The reaction mixtures were cured in air at 60 °C for 2 h, then at 80 °C for 2 h, followed by 100 °C for 20 h, and subsequently postcured under vacuum at 100 °C for 48 h.

Fourier transform infrared (FTIR) spectra for NIPU networks

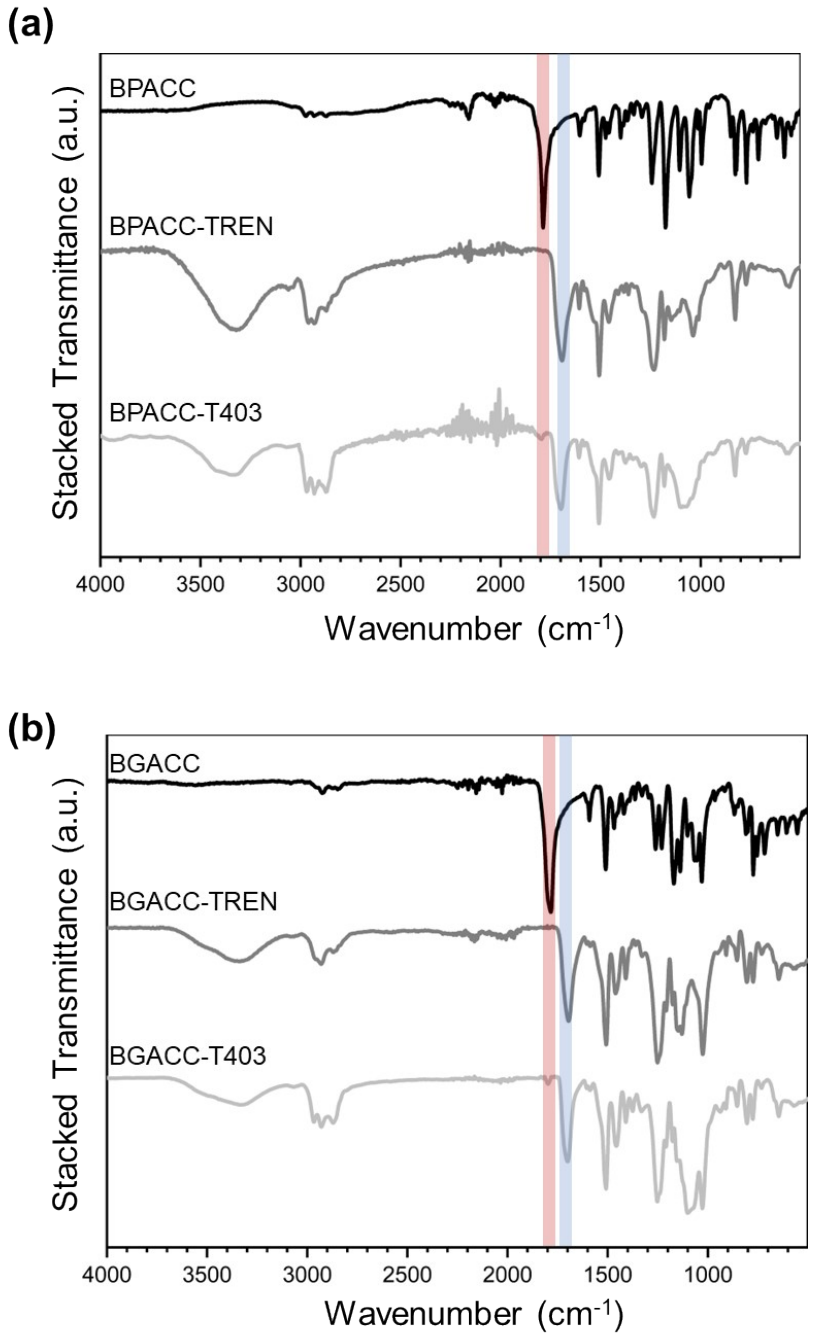

Figure S12. Stacked FTIR spectra of (a) BPACC, BPACC-TREN, and BPACC-T403, and (b) BGACC, BGACC-TREN, and BGACC-T403. The conversion was probed qualitatively by the disappearance of the cyclic carbonate carbonyl stretching band at ~1790 cm^{-1} (highlighted in red), the appearance of the urethane carbonyl stretching band at ~1700 cm^{-1} (highlighted in blue), and the appearance of the hydroxyl stretching band at ~3500–3300 cm^{-1}. Curves are shifted vertically for clarity.

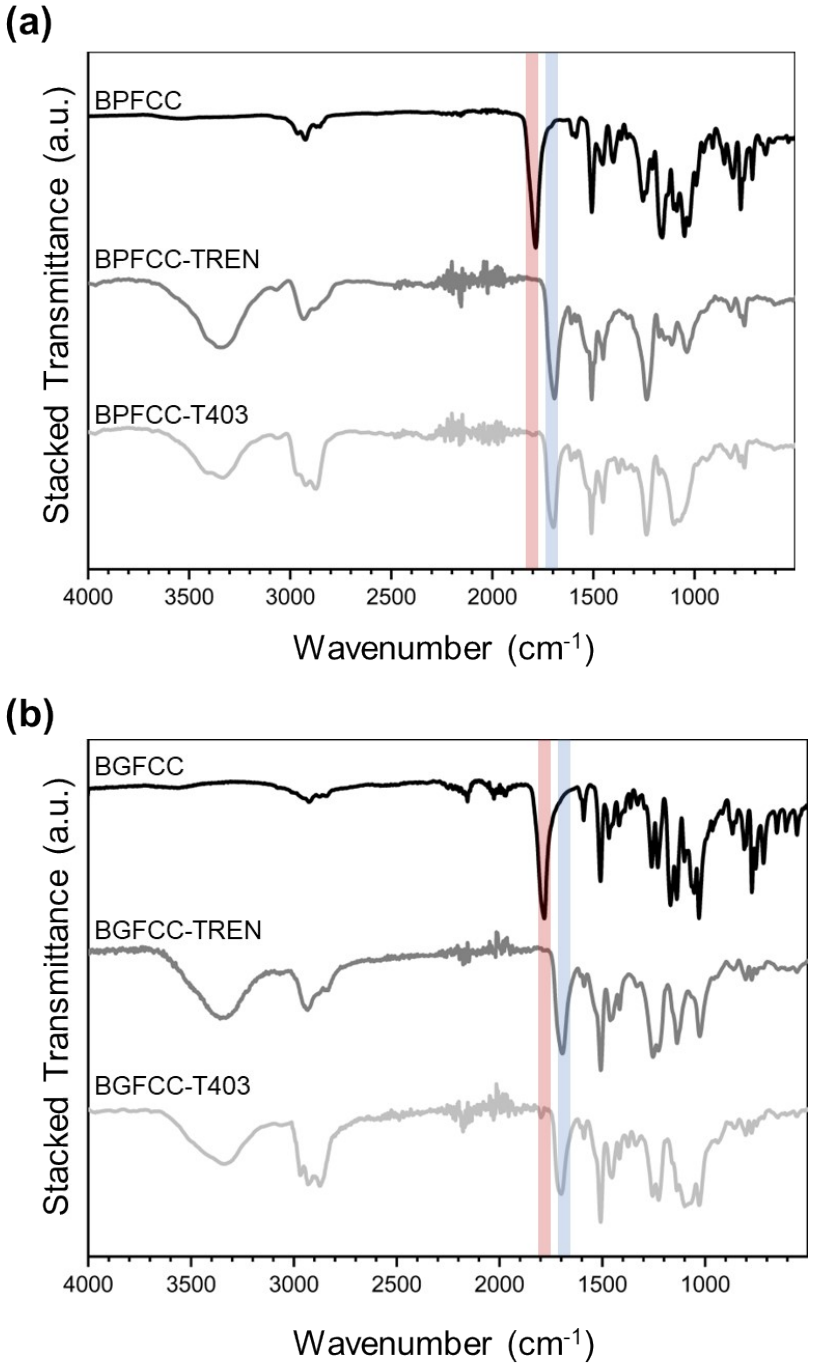

Figure S13. Stacked FTIR spectra of (a) BPFCC, BPFCC-TREN, and BPFCC-T403, and (b) BGFCC, BGFCC-TREN, and BGFCC-T403. The conversion was probed qualitatively by the disappearance of the cyclic carbonate carbonyl stretching band at ~1790 cm^{-1} (highlighted in red), the appearance of the urethane carbonyl stretching band at ~1700 cm^{-1} (highlighted in blue), and the appearance of the hydroxyl stretching band at ~3500–3300 cm^{-1}. Curves are shifted vertically for clarity.

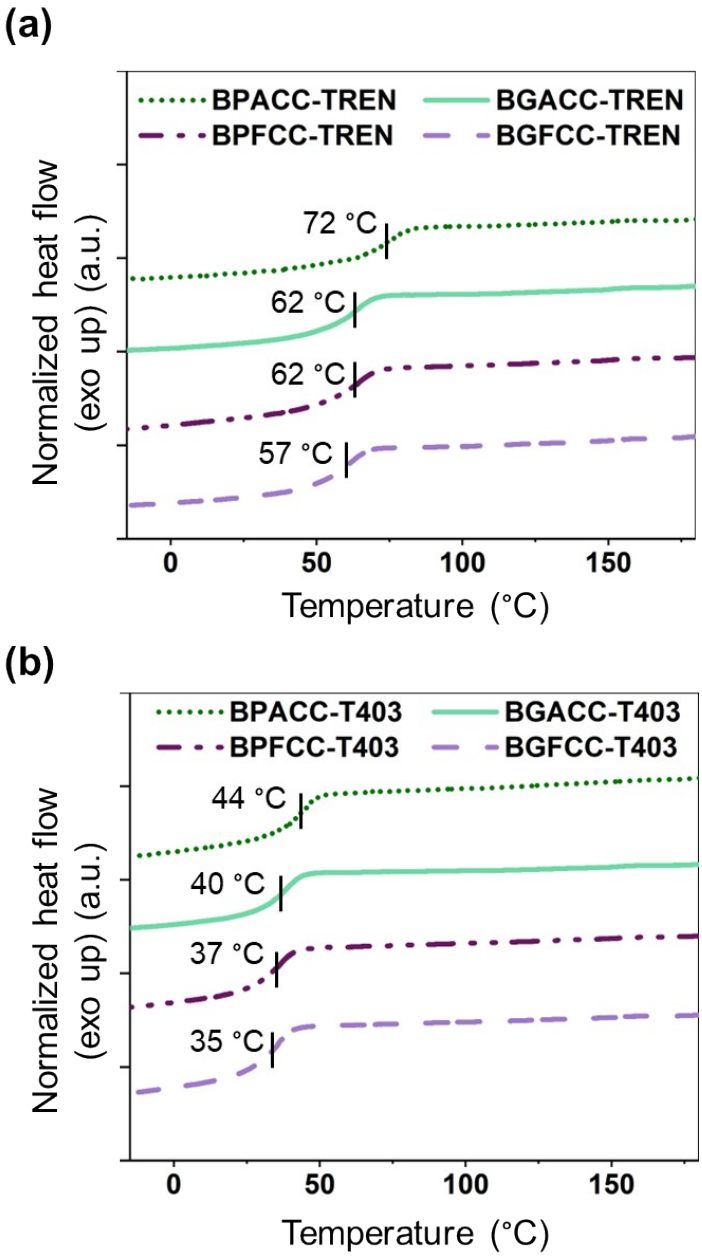

Figure S14. Representative differential scanning calorimetry (DSC) first cooling traces of (a) TREN-based and (b) T403-based NIPU networks (10 °C/min under an N_2 atmosphere). Curves are shifted vertically for clarity with glass transition temperature (T_g) values marked on the respective curves. Each tick mark on the y-axis represents a 0.2 W/g increment.

Table S1. T_g and excess enthalpy values of NIPU networks from DSC data

Sample	Excess enthalpy (J/g)[a,b]	T_g (°C)[b,c]
BPACC-TREN	0.52 ± 0.15	72 ± 0.4
BGACC-TREN	0.44 ± 0.07	62 ± 0.2
BPFCC-TREN	0.46 ± 0.15	62 ± 0.4
BGFCC-TREN	0.50 ± 0.12	57 ± 1.8
BPACC-T403	0.52 ± 0.13	42 ± 1.7
BGACC-T403	0.52 ± 0.03	40 ± 0.6
BPFCC-T403	0.44 ± 0.07	37 ± 0.5
BGFCC-T403	0.54 ± 0.01	35 ± 0.6

[a]Determined from the magnitude of the area under the peaks associated with physical aging from the second heating traces of DSC at a heating rate of 10 °C/min in an N_2 atmosphere.
[b]The reported values are the average of three repeats with errors representing the standard deviation.
[c]Determined from the first cooling trace of DSC at a cooling rate of 10 °C/min in an N_2 atmosphere.

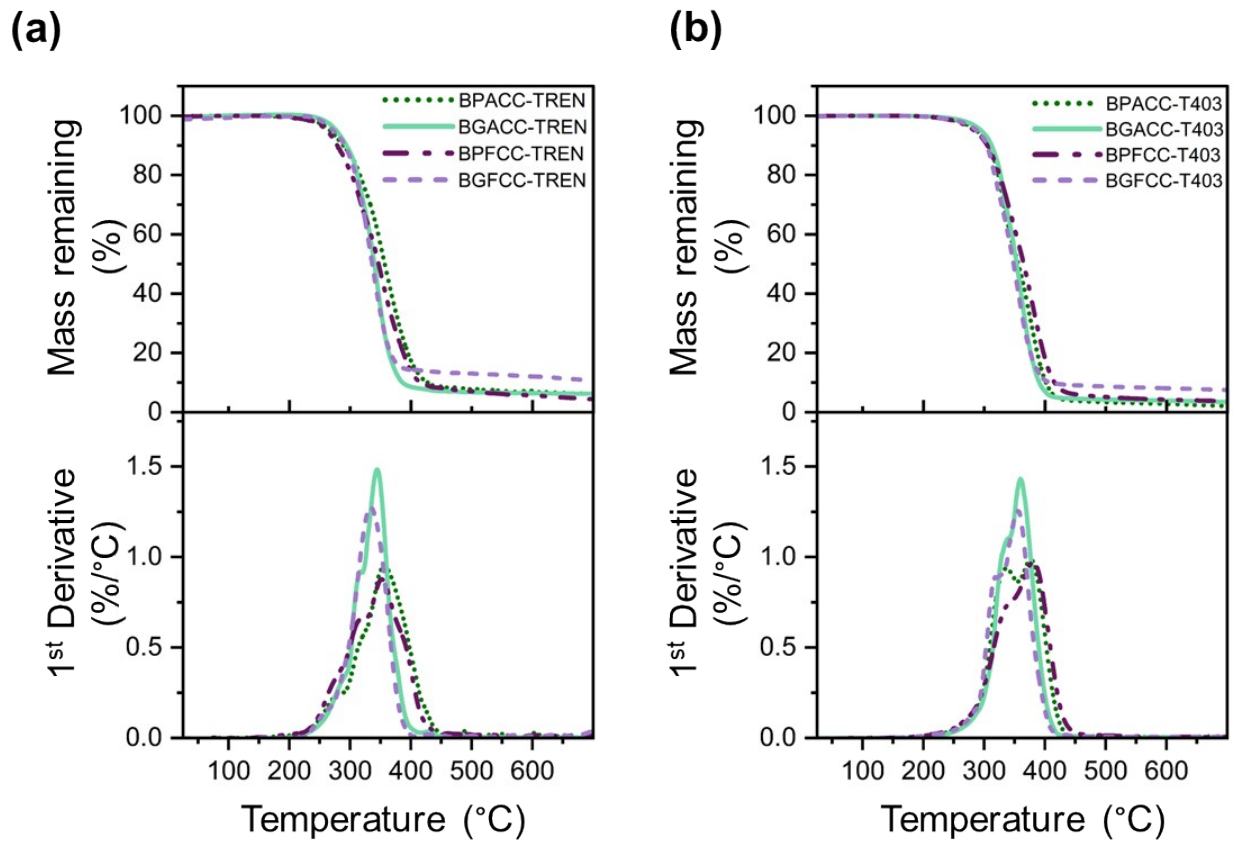

Figure S15. Representative thermogravimetric analysis traces and the respective first-derivative curves of sample mass remaining *versus* temperature for (a) TREN-based and (b) T403-based NIPU networks obtained at a heating rate of 10°C/min in an N_2 atmosphere.

Table S2. T_g and tan δ values of NIPU networks from dynamic mechanical analysis (DMA)

Sample	T_g (°C)[a,b]	tan δ[b,c]
BPACC-TREN	96 ± 2	1.3 ± 0.1
BGACC-TREN	84 ± 1	2.3 ± 0.1
BPFCC-TREN	88 ± 1	2.2 ± 0.1
BGFCC-TREN	83 ± 1	1.9 ± 0.2
BPACC-T403	55 ± 0	2.2 ± 0.2
BGACC-T403	54 ± 1	2.6 ± 0.1
BPFCC-T403	52 ± 3	2.2 ± 0.2
BGFCC-T403	51 ± 1	2.1 ± 0.2

[a] T_g values are the temperature of the maximum tan δ from the second heating trace of DMA experiments conducted in oscillatory film-tension mode at a heating rate of 3 °C/min, strain amplitude of 0.3%, frequency of 0.1 Hz, and an axial force of 0.4 N.
[b] The reported values are the average of three repeats with errors representing the standard deviation.
[c] tan δ values are obtained from the height of the tan δ peaks from the second heating trace of DMA experiments.

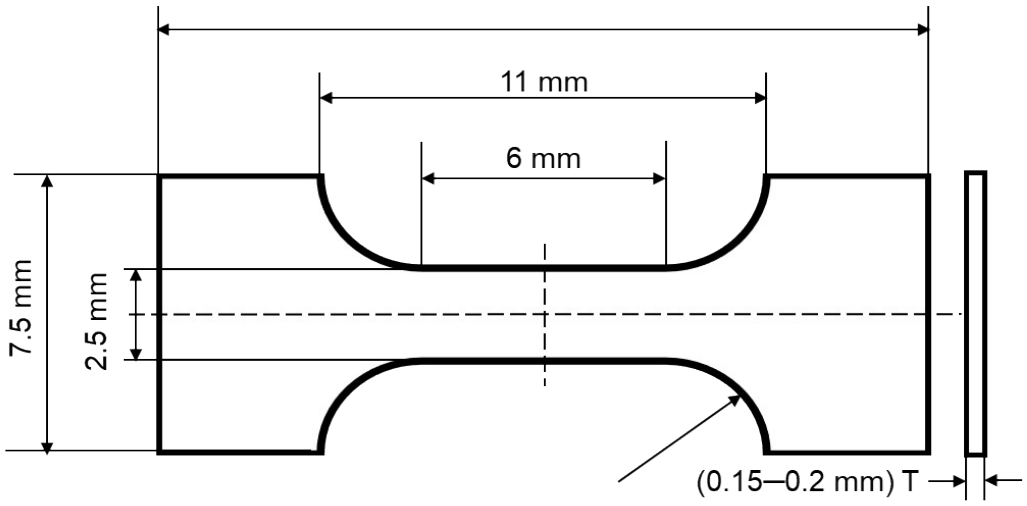

Figure S16. Dimensions of the NIPU networks used for tensile testing

Table S3. Young's modulus (E_o) values of NIPU networks

Sample	E_o (GPa)[a,b]
BPACC-TREN	2.0 ± 0.3
BGACC-TREN	2.1 ± 1.3
BPFCC-TREN	2.0 ± 0.3
BGFCC-TREN	1.7 ± 0.3
BPACC-T403	2.2 ± 0.7
BGACC-T403	2.2 ± 1.3
BPFCC-T403	1.4 ± 0.6
BGFCC-T403	1.2 ± 0.4

[a]Young's modulus was determined from the slope of the initial elastic region in the engineering tensile stress-strain curves. All data are based on tensile stress-strain curves obtained from the uniaxial tensile testing using a load cell of 100 N and an extension rate of 10 mm/min at ~20 °C.
[b]The reported values are the average of five repeats with errors representing the standard deviation.

Water uptake studies

The equilibrium water uptake of NIPU thermoset films was estimated using an accelerated test to understand if the films had different moisture uptake, which could affect the realtive tensile properties. A representative sample of each NIPU thermoset film (~60 mg) was weighed and placed at ~20 °C in a 20-mL scintillation vial filled with 15 mL of deionized (DI) water. Next, the samples were removed from the vial after 24 h, quickly patted with KimWipe™, and weighed. The specimens were then placed back in the vials for an additional 24 h and reweighed. Those final (48 h) weights were used to determine the water uptake values in **Table S4**. The water uptake was estimated by $(m_{wet} - m_0)/m_0$, for which m_{wet} and m_0 are the weight of the hydrated sample and the initial weight of the sample, respectively. Three repeats were performed for each sample, and the reported values are the average water uptake with errors representing the standard deviations.

Table S4. Water uptake values of NIPU networks

Sample	Water uptake (%)[a]
BPACC-TREN	3.2 ± 0.3
BGACC-TREN	3.1 ± 0.2
BPFCC-TREN	2.5 ± 0.9
BGFCC-TREN	3.1 ± 0.3
BPACC-T403	2.9 ± 0.7
BGACC-T403	3.9 ± 0.3
BPFCC-T403	2.8 ± 0.2
BGFCC-T403	5.4 ± 0.9

[a]The reported values are the average of three repeats with errors representing the standard deviation.

Abbreviations

BGACC	Bisguaiacol A cyclic carbonate
BGFCC	Bisguaiacol F cyclic carbonate
BPACC	Bisphenol A cyclic carbonate
BPFCC	Bisphenol F cyclic carbonate
DI	Deionized
DMA	Dynamic mechanical analysis
DMSO-d_6	Deuterated dimethyl sulfoxide
DSC	Differential scanning calorimetry
E_o	Young's modulus
FTIR	Fourier transform infrared
NIPU	Non-isocyanate polyurethane
NMR	Nuclear magnetic resonance
T403	Jeffamine® T-403
T_g	Glass transition temperature
TREN	Tris(2-aminoethyl) amine